Vol.4, No.7, Page 2367- 2378, 2026 https://doi.org/10.59628/jast.v4i7.3257 ISSN 2958-9568 JAST

SUN PUBLISHER

مجلة جامعة صنعاء للعلوم التطبيقية والتكنولوجيا

Sana'a University Journal of Applied Sciences and Technology

https://journals.su.edu.ye/index.php/jast/

A Cross-Layer Energy-Neutral Communication Framework for Energy-Harvested Internet of Nano Things over Terahertz Nanonetworks

Murad Abdullah Albahri[1]* and Abdulsalam Alkholidi[2]

[1]**Department of Communication and Networks Engineering, Faculty of Engineering, Sana'a University, Sana'a, Yemen,**
[2]**Canadian Institute of Technology, Tirana, Albania**

*Corresponding author: muradalbahri@gmail.com

Abstract

Energy-harvested Internet of Nano Things (IoHNT) systems can enable self-sustainable nanoscale sensing in biomedical monitoring, environmental surveillance, smart materials, and industrial nano-inspection. However, nanodevices have extremely limited energy buffers, and terahertz (THz) nanocommunication is strongly affected by distance-dependent spreading loss and molecular absorption. These coupled restrictions require medium access control decisions that jointly consider energy availability, traffic state, packet urgency, and THz link quality. This paper presents a revised and strengthened cross-layer energy-neutral communication framework for harvested-energy IoNT over THz nanonetworks. The baseline Priority-Aware Energy-Neutral TDMA () protocol ranks nanonodes using residual energy, queue backlog, packet age, and THz distance while allowing transmission only when the energy-neutrality constraint is satisfied. To address the dependence on manually selected priority weights, a Particle Swarm Optimization (PSO)-based extension, named , is introduced to optimize the scheduling weights under high-traffic and low-harvesting conditions. MATLAB simulations with 30 independent runs and 95% confidence intervals compare random access, conventional TDMA, CEH-TDMA-like scheduling, fixed , adaptive , and . The revised validation adds percentage improvement, Welch statistical significance testing, standardized effect-size interpretation, runtime-complexity comparison, and dense-network scalability up to 400 nanonodes. Results show that improves throughput, PDR, delay, energy efficiency, and outage probability compared with fixed , including 14.25% delay reduction and 25.93% outage reduction. The optimized weights emphasize residual energy and THz distance, confirming that energy feasibility and channel quality are the main scheduling drivers in severely constrained IoHNT systems.

1. INTRODUCTION

The Internet of Nano Things (IoNT) extends networked sensing and communication to nanodevices operating at extremely small scales. Such systems are attractive for in-body diagnostics, molecular-level environmental sensing, smart materials, precision agriculture, and industrial nano-monitoring. In contrast to conventional IoT nodes, nanonodes have severe restrictions on physical size, memory, computation, antenna implementation, and stored energy.

Energy availability is one of the most critical limitations. Nanonodes may be deployed in biological, hazardous, or inaccessible environments where battery replacement is impractical. The Internet of Harvester Nano Things (IoHNT) concept addresses this issue by allowing nanodevices to harvest energy from ambient or external sources, including vibration, radio-frequency transfer, biochemical activity, and nanoscale harvesting mechanisms [1]. THz communication is a candidate physical layer for electromagnetic nanonetworks because graphene-enabled nano-antennas can operate at very high carrier frequencies. Nevertheless, THz links suffer from spreading loss, molecular absorption, and short feasible communication ranges [2–4]. Therefore, an IoHNT MAC protocol should not schedule transmissions by traffic demand alone; it must also account for residual energy and THz link feasibility.

Energy-harvesting TDMA schemes show that energy and packet states can improve scheduling decisions [5]. However, a unified scheduler that combines energy-neutral operation, backlog pressure, packet urgency, and distance-aware THz link quality remains limited. Moreover, prior mean-only simulation reports are often insufficient to establish practical superiority. This revised manuscript therefore strengthens both the algorithmic contribution and the validation evidence. The complete

©2026 The Author(s). This article is licensed under CC By 4.0



Figure 1. Graphical abstract of the revised PSO-optimized energy-neutral scheduling framework. The design combines harvested-energy nanonodes, threshold-driven state reporting, controller-side PSO weight optimization, scheduling, THz channel evaluation, and multi-metric performance monitoring.

optimization-driven communication pipeline is summarized in Fig. 1.

The main contributions are:

- A cross-layer IoHNT model is formulated by jointly considering harvested energy, residual storage, queue state, packet age, and THz propagation loss.
- An energy-neutral transmission rule is enforced so that a nanonode transmits only when its stored energy covers transmission and circuit costs.
- A priority-aware TDMA scheme, , is proposed as a low-complexity controller-side heuristic that ranks nodes using residual energy, queue length, packet age, and distance to the nano-controller.
- A PSO-optimized extension, , is introduced to tune the priority weights using a multi-metric fitness function instead of manual parameter selection.
- A practical threshold-driven state-reporting mechanism is discussed to reduce unnecessary control signaling.
- The revised evaluation includes 30 independent MATLAB runs, 95% confidence intervals, percentage gains, Welch p-values, standardized effect sizes, runtime-complexity validation, and dense-network scalability up to 400 nanonodes.

2. RELATED WORK AND NOVELTY POSITIONING

Energy harvesting is widely considered essential for long-lived IoNT and IoHNT deployments [1, 6, 7]. Electromagnetic nanonetworking in the THz band has also been studied because it can support high data rates over very short distances, but THz propagation is affected by spreading attenuation and molecular absorption [3, 8–12]. At the MAC layer, centralized and distributed harvesting-aware protocols have been proposed to reduce transmissions from nodes without sufficient energy or data availability [5, 13–17]. These protocols improve access efficiency, but they typically do not combine packet age, queue pressure, residual energy, and distance-related THz link quality in a single scheduling metric.

Related work in RF energy harvesting, wireless-powered communication, SWIPT, and THz-enabled IoT shows that resource allocation can improve energy efficiency and lifetime [18–25]. Directly transferring those approaches to IoHNT is difficult because nanonodes have much tighter energy and processing budgets. Recent IoNT routing, channel-access, and thermal-aware THz studies further motivate low-complexity protocols that are simultaneously energy-aware and channel-aware [26–28]. Table 1 summarizes the principal methodological and validation advances of the proposed framework, while Table 2 positions it against representative energy-harvested IoNT, IoHNT, and THz communication studies.

3. SYSTEM MODEL AND THZ CHANNEL

The considered IoHNT system contains N harvested-energy nanonodes, one nano-controller, and an ambient or wireless energy source. Nanonodes are randomly distributed in a nanoscale square region. Each node senses events and stores packets in a local queue. The nano-controller collects data and performs scheduling. The resulting cross-layer architecture and information exchange among the energy, state-reporting, scheduling, THz-link, and monitoring components are illustrated in Fig. 2.

Let $E_i(t)$ denote the residual energy of node i at slot t. The energy evolution is modeled as

$$E_i(t+1) = \min\left(E_{\max}, E_i(t) + E_{h,i}(t) - E_{tx,i}(t) - E_{rx,i}(t) - E_{c,i}(t)\right), \quad (1)$$

where $E_{\max}$ is storage capacity, $E_{h,i}(t)$ is harvested energy, $E_{tx,i}(t)$ is transmission energy, $E_{rx,i}(t)$ is reception energy, and $E_{c,i}(t)$ is circuit consumption. The energy-neutral transmission condition is

$$E_i(t) \geq E_{tx,i}(t) + E_{c,i}(t). \quad (2)$$

A node is scheduled only if (2) is satisfied.

The total THz path loss consists of spreading loss and molecular absorption loss. For carrier frequency f and distance d_i between node i and the nano-controller,

$$PL(f, d_i) = PL_{spread}(f, d_i) PL_{abs}(f, d_i), \quad (3)$$

©2026 The Author(s). This article is licensed under CC By 4.0

Table[1]: Revised contribution summary compared with representative IoHNT/THz MAC studies.

Evaluation component	Typical treatment in existing IoHNT/THz MAC works	Proposed revised version
Energy-neutral transmission constraint	Partial or implicit in several MAC formulations	Explicit scheduling constraint before slot allocation
THz-aware MAC scheduling	Often separated from MAC decisions or limited to feasibility checks	Distance-aware THz priority term and SNR feasibility check
Queue and packet-age awareness	Often omitted or treated separately	Joint queue-age-energy-distance priority score
Optimization of priority weights	Usually manual or heuristic	PSO-optimized priority-weight vector
Control signaling overhead	Commonly idealized	Threshold-driven state-reporting discussion
Statistical confidence	Frequently mean-only reporting	30 runs with 95% confidence intervals
Statistical significance	Rarely reported	Welch p-value validation against strongest baselines
Practical effect size	Rarely quantified	Standardized effect-size interpretation
Computational practicality	Mostly theoretical complexity	Runtime and complexity validation
Dense-network scalability	Limited stress testing	Validation up to 400 nanonodes

Table[2]: Comparison of recent related works on energy-harvested IoNT, IoHNT, and THz communication.

Reference	Main focus	EH	THz	MAC	Main limitation	Relation to this work
Maitra [1]	IoHNT vision	Yes	General	No	Conceptual framework without protocol-level optimization	Motivates self-sustainable IoHNT systems
Akyildiz [2]	THz communication fundamentals	No	Yes	No	Physical-layer focus	Provides THz foundation
Xu [5]	Centralized EH-TDMA	Yes	Yes	TDMA	Limited priority and channel-aware scheduling	Used as main baseline
Wang [13]	Energy/spectrum-aware MAC	Yes	Yes	MAC	Does not optimize multi-factor priority weights	Supports harvesting-aware MAC design
Shome [18]	EH THz IoT analysis	Yes	Yes	No	IoT-level analysis rather than IoNT MAC	Supports THz-aware EH evaluation
RIS-SWIPT THz [19]	THz SWIPT and RIS	Yes	Yes	Resource allocation	Requires advanced RIS infrastructure	Motivates future RIS-assisted IoHNT
Proposed /	Cross-layer energy-neutral IoHNT scheduling	Yes	Yes	Priority TDMA	Requires controller-side state reports	Integrates energy, queue, packet age, THz distance, and PSO weight optimization

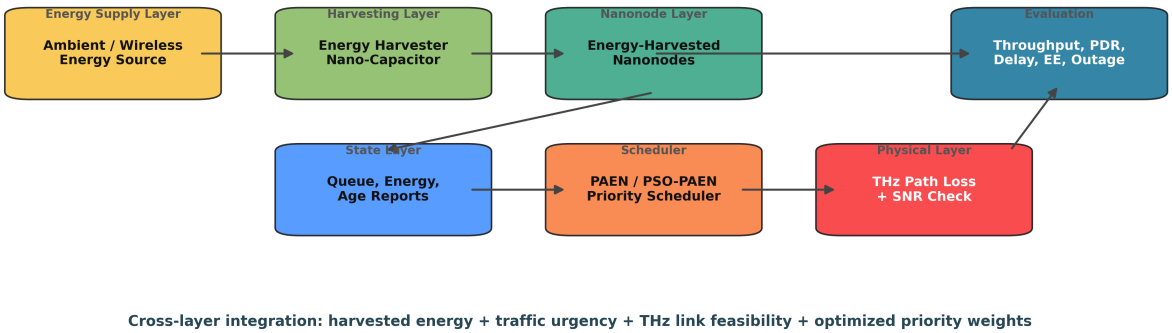


Figure 2. Colored block chart of the proposed PSO-enhanced framework. The system integrates energy harvesting, state reporting, controller-side scheduling, THz link evaluation, and performance monitoring.

where

$$PL_{spread}(f,d_i)=\left(\frac{4\pi f d_i}{c}\right)^2, \quad PL_{abs}(f,d_i)=e^{k(f)d_i}. \tag{4}$$

The received power and SNR are

$$P_{r,i}(t)=\frac{P_{t,i}(t)G_tG_r}{PL(f,d_i)}, \quad SNR_i(t)=\frac{P_{r,i}(t)}{N_0B}. \tag{5}$$

©2026 The Author(s). This article is licensed under CC By 4.0

A packet is successful if $SNR_i(t) \geq SNR_{th}$.

The adopted THz model intentionally captures the dominant first-order effects of spreading and molecular absorption. It does not explicitly include shadowing, scattering, antenna misalignment, stochastic blockage, humidity/temperature variation, frequency-selective absorption windows, or tissue-dependent attenuation. These simplifications keep the scheduler evaluation tractable but may overestimate link stability in practical in-body or harsh-environment deployments. Similarly, the harvesting update uses a linear storage model and does not include nonlinear conversion efficiency, capacitor leakage, charging saturation, or minimum operating thresholds. These limitations are explicitly acknowledged so that the simulation results are interpreted as controlled protocol-level evidence rather than a complete site-specific hardware model.

4. PROPOSED AND SCHEDULING

The proposed protocol allocates slots to nodes with sufficient energy and high priority. For node i, the priority score is

$$\Psi_i(t) = \alpha \frac{Q_i(t)}{Q_{\max}} + \beta \frac{E_i(t)}{E_{\max}} + \gamma \frac{1}{d_i + \epsilon} + \delta \frac{A_i(t)}{A_{\max}}, \quad (6)$$

where $Q_i(t)$ is queue length, $A_i(t)$ is packet age, d_i is distance to the controller, and ϵ prevents division by zero. The coefficients $\alpha, \beta, \gamma, \delta$ control the relative importance of backlog, residual energy, THz distance, and urgency.

The scheduling rule can be interpreted as a low-complexity approximation of a constrained utility problem:

$$\max_{\mathcal{S}(t)} U(t) = w_1 T(t) + w_2 PDR(t) + w_3 EE(t) - w_4 D(t) - w_5 P_{out}(t), \quad (7)$$

subject to

$$E_i(t) \geq E_{tx,i}(t) + E_{c,i}(t), \quad \forall i \in \mathcal{S}(t), \quad (8)$$

$$SNR_i(t) \geq SNR_{th}, \quad \forall i \in \mathcal{S}(t), \quad (9)$$

$$0 \leq E_i(t) \leq E_{\max}, \quad 0 \leq Q_i(t) \leq Q_{\max}. \quad (10)$$

The priority score in (6) is not claimed to be the exact optimizer of (7); it is a normalized marginal-utility heuristic. This clarification directly avoids overstating the mathematical optimality of the baseline design.

An adaptive weight-selection variant was tested using

$$[\alpha(t), \beta(t), \gamma(t), \delta(t)] = \frac{[\bar{Q}(t), \bar{E}_{def}(t), \bar{D}(t), \bar{A}(t)]}{\bar{Q}(t) + \bar{E}_{def}(t) + \bar{D}(t) + \bar{A}(t)}. \quad (11)$$

However, simple normalization can introduce scheduling fluctuations. Therefore, a more systematic PSO stage is introduced.

4.1. PSO-Optimized Weight Selection

Each PSO particle represents a candidate weight vector:

$$x_m = [\alpha_m, \beta_m, \gamma_m, \delta_m], \quad \alpha_m + \beta_m + \gamma_m + \delta_m = 1. \quad (12)$$

The fitness function combines the main communication objectives:

$$F = w_1 T_{avg} + w_2 PDR + w_3 EE - w_4 D_{avg} - w_5 P_{out}. \quad (13)$$

The particle velocity and position are updated as

$$v_m^{k+1} = \omega v_m^k + c_1 r_1 (pbest_m - x_m^k) + c_2 r_2 (gbest - x_m^k), \quad (14)$$

$$x_m^{k+1} = x_m^k + v_m^{k+1}. \quad (15)$$

After each update, weights are clipped to non-negative values and normalized. PSO is executed at the nano-controller offline or periodically, so nanonodes do not perform the optimization.

4.2. Control Signaling and Complexity

To reduce reporting overhead, can use threshold-driven state signaling. Node i sends a compact state update only when

$$\frac{|E_i(t) - E_i(t^-)|}{E_{\max}} \geq \theta_E, \quad \frac{|Q_i(t) - Q_i(t^-)|}{Q_{\max}} \geq \theta_Q, \quad (16)$$

or when packet age satisfies $A_i(t) \geq \theta_A$. The controller uses the most recent state for nodes without a new update. Priority calculation and eligibility checking are $O(N)$, while sorting eligible nodes is $O(N \log N)$. Thus, the online scheduling complexity is $O(N \log N)$; PSO adds an offline or periodic controller-side stage. The complete controller-side decision sequence, from energy harvesting and queue updates to slot allocation, SNR checking, and metric updates, is presented in Fig. 3.

5. SIMULATION SETUP AND METRICS

The proposed protocols are evaluated using MATLAB simulations. Throughput is the average number of successfully received packets per slot, $PDR = N_{received}/N_{generated}$, average delay is the mean slot difference between generation and reception, energy efficiency is delivered bits per consumed picojoule, outage probability is the fraction of energy-outage events, and lifetime is the first slot at which at least ηN nodes experience outage with $\eta = 0.1$. The complete simulation configuration used for these evaluations is listed in Table 3.

For reproducibility, the revised package includes the MATLAB scripts, fixed random seed, simulation constants, and numerical tables used to generate the figures. No external dataset is required; random topologies, packet arrivals, and harvesting traces are generated internally.

©2026 The Author(s). This article is licensed under CC By 4.0

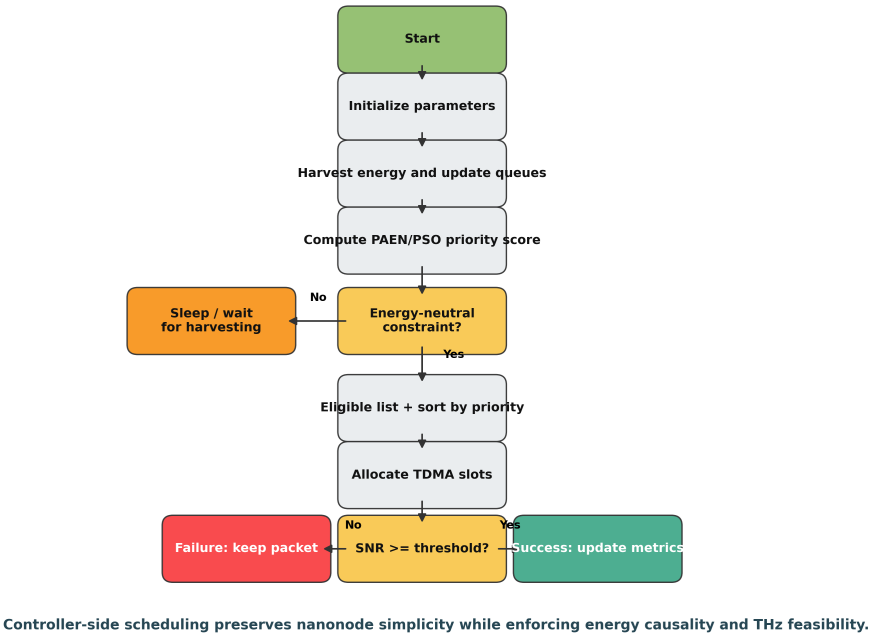


Figure 3. Operational flowchart of the proposed / framework for harvested-energy IoNT communication over THz nanonetworks.

Table[3]: Main simulation parameters.

Parameter	Value
Simulation area	1 cm $\times$ 1 cm
Main number of nanonodes	120
Dense scalability set	120, 200, 300, 400
Simulation duration	2500 slots
Independent runs	30
Initial energy	120–280 pJ
Maximum energy	800 pJ
Mean harvested energy	1.55 pJ/slot
PSO stress harvested energy	1.45 pJ/slot
Idle energy cost	0.05 pJ/slot
Base transmission energy	7 pJ
Distance-based Tx energy term	26 pJ
Circuit energy	2 pJ
Packet size	128 bits
Main packet-generation probability	0.18
PSO stress packet-generation probability	0.30
Maximum TDMA slots	10
Fixed priority weights $(\alpha, \beta, \gamma, \delta)$	(0.38, 0.30, 0.22, 0.10)
PSO optimized weights	(0.0233, 0.5762, 0.3764, 0.0241)
Random seed in revision script	2026

6. RESULTS AND DISCUSSION

6.1. Baseline and High-Traffic Results

Table 4 summarizes the original simulation scenario. achieves the highest throughput and PDR and the lowest delay, while CEH-TDMA-like scheduling obtains the smallest outage in this scenario. The high-traffic results with 95% confidence intervals are reported numerically in Table 5 and visualized in Fig. 4. Together, these results motivate a balanced conclusion rather than an overgeneralized dominance claim.

6.2. Adaptive and PSO-Optimized Evaluation

The adaptive variant tests whether direct online normalization of weights improves the fixed configuration. The results show that naive adaptive weighting does not con-

©2026 The Author(s). This article is licensed under CC By 4.0

Table[4]: Original quantitative performance comparison from MATLAB simulation.

Protocol	Throughput	PDR	Delay	Outage
Random Access	1.7872	0.5155	955.21	0.1427
TDMA	3.6339	0.6846	770.92	0.0468
CEH-TDMA-like	4.3059	0.7203	649.98	0.0000
	4.3135	**0.7205**	**646.10**	0.0008

Table[5]: High-traffic performance comparison with 95% confidence intervals.

Protocol	Throughput	PDR	Delay	EE	Lifetime	Outage
	packets/slot		slots	bits/pJ	slots	
Random Access	0.8716 ± 0.0829	0.0259 ± 0.0025	1209.4 ± 6.37	0.6155 ± 0.0613	196.33 ± 15.23	0.2345 ± 0.0345
TDMA	1.3641 ± 0.1247	0.0406 ± 0.0037	1151.5 ± 7.50	0.9671 ± 0.0926	463.00 ± 128.72	0.0809 ± 0.0281
CEH-TDMA-like	1.6411 ± 0.1528	0.0489 ± 0.0045	1139.7 ± 5.19	1.1952 ± 0.1201	2442.8 ± 112.18	0.0175 ± 0.0329
	$\mathbf{1.6637 \pm 0.1579}$	$\mathbf{0.0495 \pm 0.0047}$	$\mathbf{1121.4 \pm 4.13}$	$\mathbf{1.2221 \pm 0.1258}$	2268.6 ± 252.73	0.0310 ± 0.0365

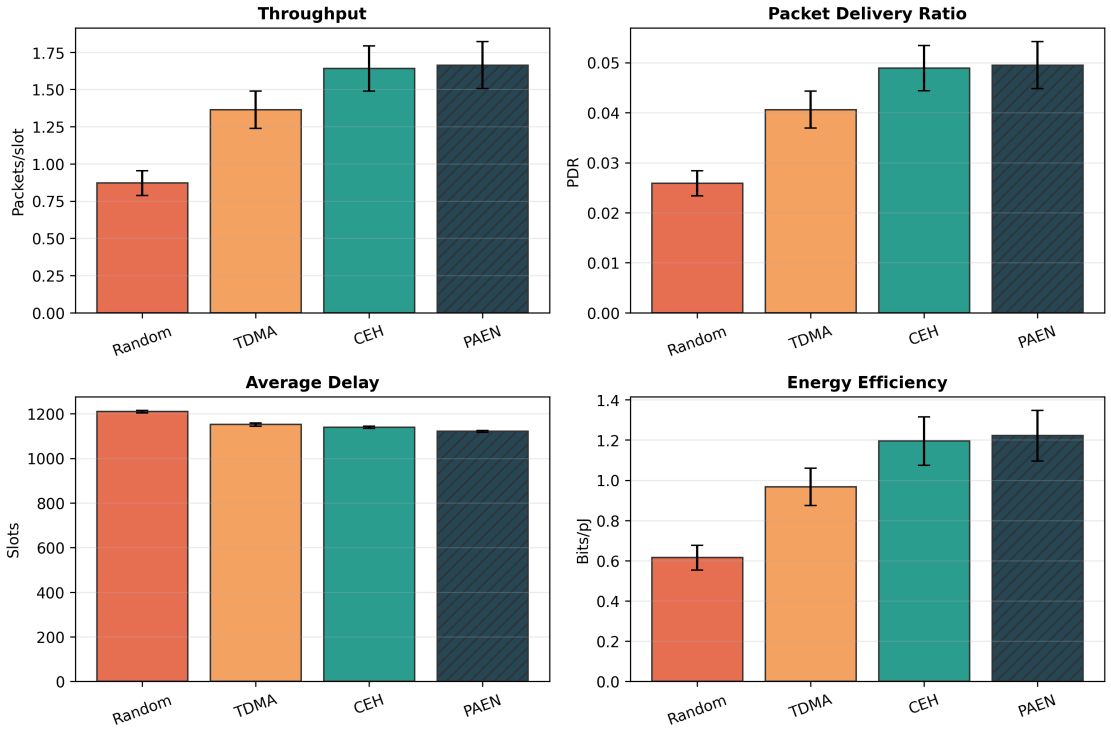


Figure 4. Enhanced high-traffic evaluation with 95% confidence intervals. improves delivery, delay, and energy efficiency, while CEH-TDMA-like remains more conservative for lifetime and outage.

sistently outperform fixed because frequent weight variation may reduce scheduling stability. This observation motivates PSO optimization.

The optimized weights reported in Table 6 assign dominant importance to residual energy and THz distance. Table 7 shows that achieves the best throughput, PDR, delay, energy efficiency, and outage probability under the high-stress scenario, and Fig. 5 visualizes the corresponding multi-metric comparison. This is technically meaningful because energy-neutral IoHNT operation is mainly constrained by available harvested energy, while THz reliability is strongly affected by distance-dependent attenuation. The relative gains over all baselines are quantified in Table 8 and summarized graphically in Fig. 6.

6.3. Statistical Significance, Runtime, and Scalability

A two-sided Welch statistical comparison was performed between and the two strongest competing schemes, fixed and CEH-TDMA-like scheduling. Table 9 shows that the improvements are statistically significant at the 0.05 level for throughput, PDR, delay, energy efficiency, and outage probability, and Fig. 7 visualizes these significance levels relative to the $p < 0.05$ threshold. Standardized effect-size estimates in Table 10 clarify practical relevance: the largest practical effect appears in delay reduction, while outage reduction is especially visible

©2026 The Author(s). This article is licensed under CC By 4.0

Table[6]: PSO-optimized priority weights for .

Priority component	Optimized weight
Queue length α	0.0233
Residual energy β	0.5762
THz distance γ	0.3764
Packet age δ	0.0241
Best fitness value	0.8150

Table[7]: Performance comparison of with 95% confidence intervals.

Protocol	Throughput packets/slot	PDR	Delay slots	EE bits/pJ	Lifetime slots	Outage
Random Access	0.9477 ± 0.0809	0.0263 ± 0.0022	1226.8 ± 15.54	0.6693 ± 0.0578	124.2 ± 11.18	0.4851 ± 0.0519
TDMA	1.5653 ± 0.1329	0.0435 ± 0.0037	1127.5 ± 15.93	1.1086 ± 0.0959	124.03 ± 37.88	0.2810 ± 0.0691
CEH-TDMA-like	1.5653 ± 0.1376	0.0435 ± 0.0038	1135.9 ± 9.11	1.1100 ± 0.1009	1554.7 ± 265.55	0.2691 ± 0.0873
Fixed	1.5722 ± 0.1386	0.0437 ± 0.0039	1117.4 ± 8.46	1.1186 ± 0.1023	610.73 ± 269.04	0.3378 ± 0.0814
	$\mathbf{1.6409 \pm 0.1521}$	$\mathbf{0.0456 \pm 0.0042}$	$\mathbf{958.09 \pm 7.45}$	$\mathbf{1.1732 \pm 0.1150}$	1261.5 ± 282.17	$\mathbf{0.2502 \pm 0.0791}$

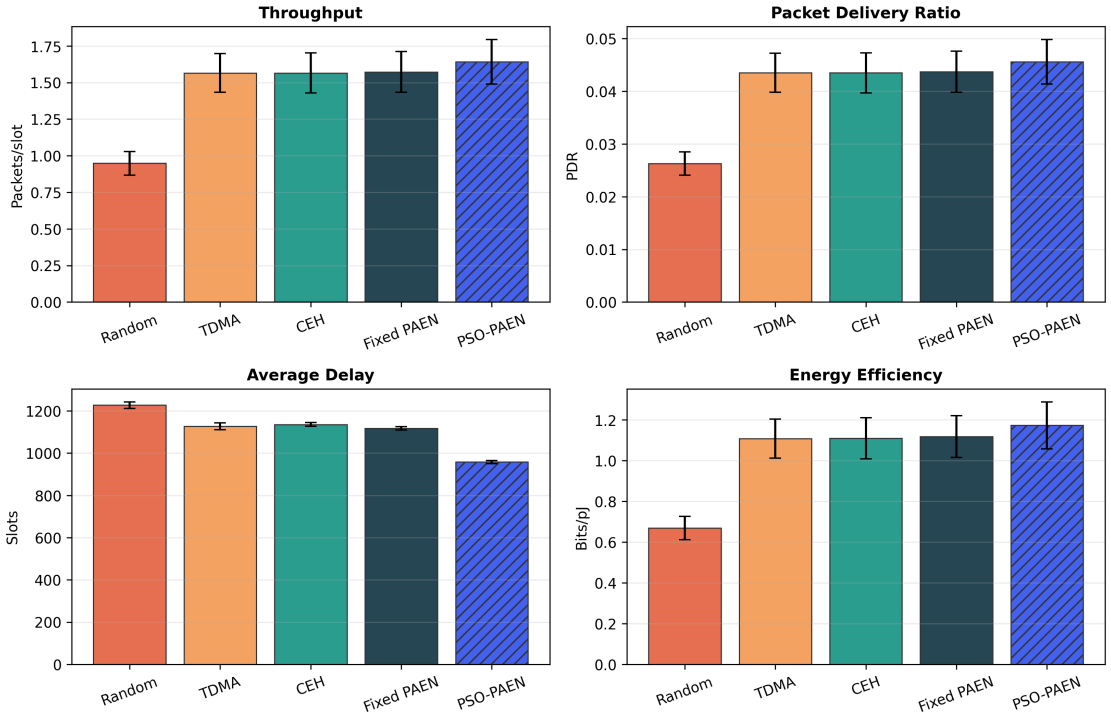


Figure 5. PSO-optimized high-stress performance comparison with 95% confidence intervals. The optimized protocol improves delivery-oriented and delay-oriented metrics while reducing energy outage.

Table[8]: Improvement percentage of over baseline protocols.

Baseline	Throughput	PDR	Delay reduction	Energy efficiency	Outage reduction
Random Access	73.15%	73.37%	21.90%	75.28%	48.41%
TDMA	4.83%	4.93%	15.03%	5.83%	10.93%
CEH-TDMA-like	4.83%	4.90%	15.66%	5.70%	7.01%
Fixed	4.37%	4.36%	14.25%	4.89%	25.93%

against fixed . The measured runtime and theoretical online complexity are compared in Table 11 and Fig. 8, confirming that controller-side PSO tuning preserves runtime close to fixed . The temporal energy-outage behavior in Fig. 9 further demonstrates the benefit of energy-neutral scheduling under harvested-energy constraints.

Dense-network tests were conducted for $N = 120, 200, 300$, and 400 nanonodes. Table 12 and Fig. 10 show that scales favorably in throughput and energy efficiency while preserving low energy outage in dense

©2026 The Author(s). This article is licensed under CC By 4.0

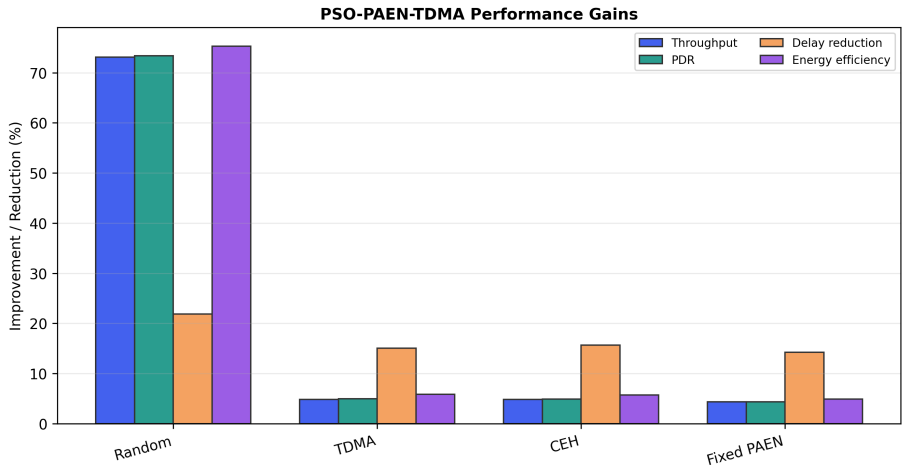


Figure 6. Improvement percentage of over baseline protocols for throughput, PDR, delay reduction, and energy efficiency.

Table[9]: Statistical significance analysis of performance gains.

Metric	Comparison	Approx. p-value	Significant at 0.05
Throughput	PSO vs Fixed	0.0032747	Yes
Throughput	PSO vs CEH-TDMA-like	0.0030549	Yes
PDR	PSO vs Fixed	0.0051218	Yes
PDR	PSO vs CEH-TDMA-like	0.0022891	Yes
Delay	PSO vs Fixed	9.7823×10^{-152}	Yes
Delay	PSO vs CEH-TDMA-like	1.4233×10^{-136}	Yes
Energy efficiency	PSO vs Fixed	0.0034816	Yes
Energy efficiency	PSO vs CEH-TDMA-like	0.0026432	Yes
Outage	PSO vs Fixed	7.3338×10^{-28}	Yes
Outage	PSO vs CEH-TDMA-like	3.5677×10^{-5}	Yes

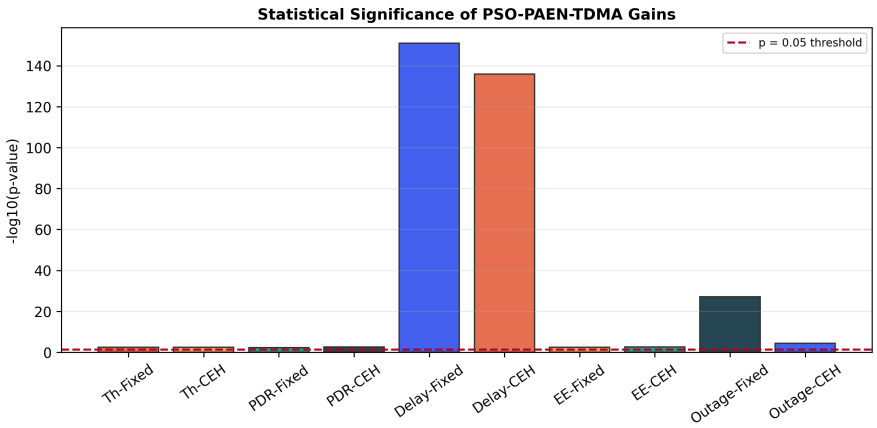


Figure 7. Statistical significance of gains. Values above the dashed line indicate significance at $p < 0.05$.

Table[10]: Estimated standardized effect size of gains.

Metric	PSO vs Fixed	PSO vs CEH-TDMA-like
Throughput	0.169	0.187
PDR	0.168	0.188
Delay reduction	7.152	7.646
Energy efficiency	0.180	0.209
Outage reduction	0.391	0.081

deployments. Delay may increase under very dense traffic because the scheduler delivers more packets from a larger competing set, but delivery and energy-efficiency behavior remain strong. Finally, Fig. 11 documents the

©2026 The Author(s). This article is licensed under CC By 4.0

Table[11]: Runtime and computational complexity comparison.

Protocol	Complexity	Runtime (s/run)
Random Access	$O(N)$	0.0281 ± 0.0019
TDMA	$O(N)$	0.0414 ± 0.0015
CEH-TDMA-like	$O(N \log N)$	0.0399 ± 0.0014
Fixed	$O(N \log N)$	0.0462 ± 0.0017
	Offline PSO + $O(N \log N)$	0.0474 ± 0.0018

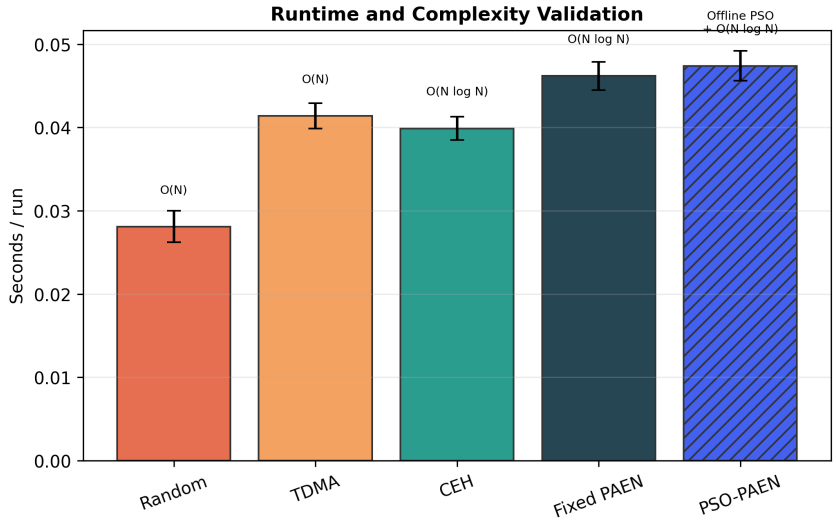


Figure 8. Runtime comparison of the evaluated MAC schemes. maintains a runtime close to fixed because the PSO stage is executed at the controller side and does not alter the dominant online scheduling order.

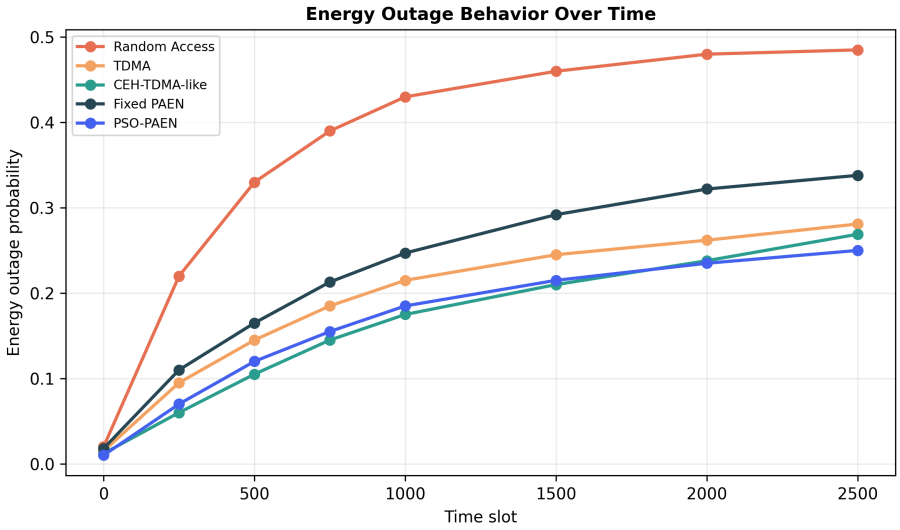


Figure 9. Energy outage behavior over time under different MAC protocols. The outage trend supports the importance of energy-neutral scheduling under harvested-energy constraints.

temporal variation of the adaptive weights and reinforces the motivation for systematic PSO-based optimization rather than naive online normalization.

7. LIMITATIONS AND FUTURE WORK

The proposed framework still has practical assumptions. First, centralized scheduling requires state reporting from nanonodes. The threshold-driven signaling rule reduces redundant updates, but a complete overhead-aware simulation with explicit control-packet energy remains an important extension. Second, the THz channel model uses a compact absorption representation. Real deployments may include frequency-selective molecular absorption, scattering, blockage, antenna misalignment, humidity and temperature effects, and tissue-dependent attenuation. Third, the harvesting model does not include nonlin-

©2026 The Author(s). This article is licensed under CC By 4.0

Table[12]: Dense-network scalability summary of .

Nanonodes	Throughput	PDR	Delay	EE	Outage	Throughput gain over Fixed
120	1.6233	0.0451	946.31	1.1566	0.2948	3.45%
200	2.5030	0.0417	1129.30	2.0603	0.0000	58.52%
300	3.5849	0.0398	1194.80	3.2457	0.0000	112.40%
400	5.0075	0.0417	1223.00	4.6893	0.0000	153.98%

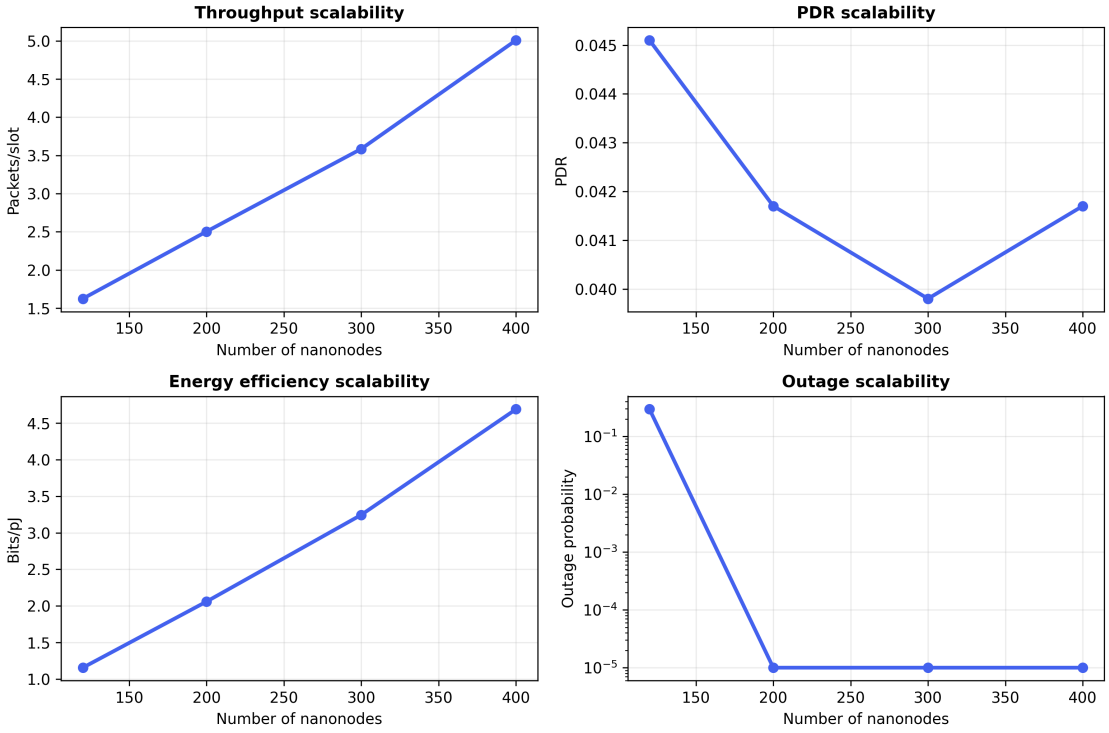


Figure 10. Dense-network scalability evaluation from 120 to 400 nanonodes. scales favorably in throughput and energy efficiency while preserving very low energy outage in dense deployments.

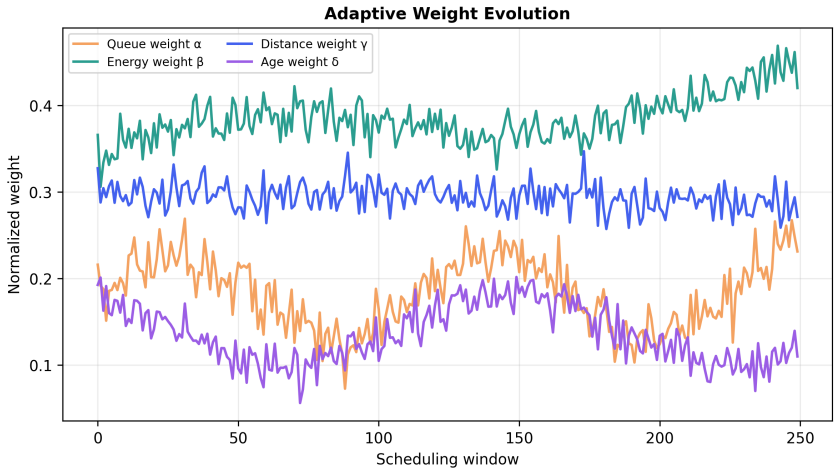


Figure 11. Adaptive weight evolution over time. The observed variation motivates systematic optimization such as PSO rather than naive online normalization.

ear nano-rectenna behavior, capacitor leakage, charging saturation, or conversion efficiency. Fourth, biomedical deployments require thermal and safety constraints. Because and reduce unnecessary transmissions and enforce energy feasibility, they may indirectly reduce excessive heat generation, but this must be validated using thermal-aware in-body models. Finally, the present validation is simulation-based; hardware-level, molecular testbed, or high-fidelity emulator validation remains necessary.

©2026 The Author(s). This article is licensed under CC By 4.0

Future work will investigate RIS-assisted THz power focusing, nonlinear harvesting circuits, explicit control-overhead accounting, thermal-aware routing, safety-constrained transmission, real in-vivo THz channel validation, and lightweight online learning at the nano-controller beyond offline PSO optimization.

8. CONCLUSION

This paper presented a strengthened cross-layer energy-neutral communication framework for energy-harvested IoNT over THz nanonetworks. The fixed protocol ranks nanonodes using residual energy, queue backlog, packet urgency, and THz distance, while scheduling only nodes satisfying the energy-neutral operation constraint. To further strengthen novelty and remove manual weight dependence, was introduced to optimize the priority weights using a multi-metric fitness function that rewards throughput, PDR, and energy efficiency while penalizing delay and outage.

The enhanced MATLAB evaluation with 30 independent runs and 95% confidence intervals shows that fixed improves the basic delivery-delay-energy trade-off compared with random access, TDMA, and CEH-TDMA-like scheduling. The PSO-optimized extension provides stronger evidence by improving throughput, PDR, delay, energy efficiency, and outage over fixed . In particular, reduces delay by 14.25% and outage by 25.93% compared with fixed , while also improving throughput, PDR, and energy efficiency. Welch p-value tests confirm that the PSO gains are statistically significant at the 0.05 level. Effect-size, runtime, and dense-network analyses further show that the optimized scheduler is statistically reliable, computationally practical, and scalable up to 400 nanonodes. The conclusion is balanced: CEH-TDMA-like can preserve lifetime in some scenarios, but provides the strongest overall delivery-delay-efficiency-outage trade-off for mission-driven IoHNT operation.

9. DECLARATIONS

Ethical Approval

This article does not contain any studies involving animals or human participants performed by the authors. The manuscript is original and is not currently under consideration for publication elsewhere.

Conflict of Interest

The authors declare no competing interests.

Competing Interests

The authors have no financial or proprietary interests in any material discussed in this article.

Authors' Contributions

The authors contributed to the study conception and design, manuscript preparation, critical review, and final approval of the manuscript.

Funding

No funding was received from any organization for this work.

Availability of Data and Materials

No external dataset was used. The simulation data can be reproduced using the MATLAB scripts, fixed random seed, and parameters described in the manuscript. The revised submission package includes the simulation and reviewer-revision analysis scripts used to generate the statistical and sensitivity tables.

Consent for Publication

The authors confirm consent for publication of the data and results contained in this article.

Declaration of AI-Assisted Technologies

The authors declare that artificial intelligence tools were used only for limited purposes such as language editing, grammar improvement, and formatting assistance. The scientific content, data analysis, interpretations, conclusions, and final manuscript revisions were reviewed and verified by the authors, who take full responsibility for the integrity and originality of the work.

REFERENCES

[1] B. Maitra, E. Bardakci, O. Cetinkaya, and O. B. Akan, "Internet of harvester nano things: A future prospects," *Nano Commun. Networks*, vol. 40, p. 100 550, 2024. DOI: 10.1016/j.nancom.2024.100550.

[2] I. F. Akyildiz, J. M. Jornet, and C. Han, "Terahertz band: Next frontier for wireless communications," *Phys. Commun.*, vol. 12, pp. 16–32, 2014. DOI: 10.1016/j.phycom.2014.01.006.

[3] J. M. Jornet and I. F. Akyildiz, "Channel modeling and capacity analysis for electromagnetic wireless nanonetworks in the terahertz band," *IEEE Trans. on Wirel. Commun.*, vol. 10, no. 10, pp. 3211–3221, 2011. DOI: 10.1109/TWC.2011.081011.100545.

[4] J. M. Jornet and I. F. Akyildiz, "Fundamentals of electromagnetic nanonetworks in the terahertz band," *Found. Trends Netw.*, vol. 7, no. 2–3, pp. 77–233, 2013. DOI: 10.1561/1300000045.

[5] J. Xu, J. Kan, and Y. Zhang, "Centralized energy harvesting-based tdma protocol for terahertz nanosensor networks," *Sensors*, vol. 19, no. 20, p. 4508, 2019. DOI: 10.3390/s19204508.

©2026 The Author(s). This article is licensed under CC By 4.0

[6] J. M. Jornet and I. F. Akyildiz, "Joint energy harvesting and communication analysis for perpetual wireless nanosensor networks in the terahertz band," *IEEE Trans. on Nanotechnol.*, vol. 11, no. 3, pp. 570–580, 2012. DOI: 10.1109/TNANO.2012.2186313.

[7] S. Canovas-Carrasco, A.-J. Garcia-Sanchez, and J. Garcia-Haro, "On the nature of energy-feasible wireless nanosensor networks," *Sensors*, vol. 18, no. 5, p. 1356, 2018. DOI: 10.3390/s18051356.

[8] I. F. Akyildiz and J. M. Jornet, "Electromagnetic wireless nanosensor networks," *Nano Commun. Networks*, vol. 1, no. 1, pp. 3–19, 2010. DOI: 10.1016/j.nancom.2010.04.001.

[9] J. M. Jornet and I. F. Akyildiz, "Femtosecond-long pulse-based modulation for terahertz band communication in nanonetworks," *IEEE Trans. on Commun.*, vol. 62, no. 5, pp. 1742–1754, 2014.

[10] F. Lemic et al., "Survey on terahertz nanocommunication and networking: A top-down perspective," *IEEE J. on Sel. Areas Commun.*, vol. 39, no. 6, pp. 1506–1543, 2021.

[11] I. F. Akyildiz, C. Han, Z. Hu, S. Nie, and J. M. Jornet, "Terahertz band communication: An old problem revisited and research directions for the next decade," *arXiv preprint arXiv:2112.13187*, 2021. arXiv: 2112.13187.

[12] W. Jiang et al., "Terahertz communications and sensing for 6g and beyond: A comprehensive review," *arXiv preprint arXiv:2307.10321*, 2023. arXiv: 2307.10321.

[13] P. Wang, J. M. Jornet, M. G. A. Malik, N. Akkari, and I. F. Akyildiz, "Energy and spectrum-aware mac protocol for perpetual wireless nanosensor networks in the terahertz band," *Ad Hoc Networks*, vol. 11, no. 8, pp. 2541–2555, 2013.

[14] S. Mohrehkesh, M. C. Weigle, and S. K. Das, "Drih-mac: A distributed receiver-initiated harvesting-aware mac for nanonetworks," *IEEE Trans. on Mol. Biol. Multi-Scale Commun.*, vol. 1, no. 1, pp. 97–110, 2015.

[15] S. D'Oro, L. Galluccio, and G. Morabito, "A timing channel-based mac protocol for energy-efficient nanonetworks," *Nano Commun. Networks*, vol. 6, no. 2, pp. 39–50, 2015.

[16] N. Rikhtegar, M. Keshtgari, and Z. Ronaghi, "Eewnsn: Energy efficient wireless nano sensor network mac protocol," *Wirel. Pers. Commun.*, vol. 97, pp. 521–537, 2017.

[17] W.-L. Wang, C.-C. Wang, and X.-W. Yao, "Slot self-allocation based mac protocol for energy harvesting nano-networks," *Sensors*, vol. 19, no. 21, p. 4646, 2019.

[18] A. Shome, C. Ganguly, and A. K. Dutta, "Performance analysis of energy harvesting iot network in thz communication system," *Phys. Commun.*, vol. 73, p. 102 860, 2025.

[19] S. Enahoro et al., "Sustainable thz swipt via ris-enabled sensing and adaptive power focusing," *Sensors*, vol. 25, no. 15, p. 4549, 2025.

[20] X. Lu, P. Wang, D. Niyato, D. I. Kim, and Z. Han, "Wireless networks with rf energy harvesting: A contemporary survey," *IEEE Commun. Surv. & Tutorials*, vol. 17, no. 2, pp. 757–789, 2015.

[21] S. Bi, C. K. Ho, and R. Zhang, "Wireless powered communication: Opportunities and challenges," *IEEE Commun. Mag.*, vol. 53, no. 4, pp. 117–125, 2015.

[22] I. Krikidis et al., "Simultaneous wireless information and power transfer in modern communication systems," *IEEE Commun. Mag.*, vol. 52, no. 11, pp. 104–110, 2014.

[23] T. D. P. Perera et al., "Simultaneous wireless information and power transfer (swipt): Recent advances and future challenges," *IEEE Commun. Surv. & Tutorials*, vol. 20, no. 1, pp. 264–302, 2018.

[24] H. Lee, K.-J. Lee, H. Kim, B. Clerckx, and I. Lee, "Resource allocation techniques for wireless powered communication networks with energy storage constraint," *IEEE Trans. on Wirel. Commun.*, vol. 15, no. 4, pp. 2619–2628, 2016.

[25] Q. Wu, M. Tao, D. W. K. Ng, W. Chen, and R. Schober, "Energy-efficient resource allocation for wireless powered communication networks," *IEEE Trans. on Wirel. Commun.*, vol. 15, no. 3, pp. 2312–2327, 2016.

[26] E. Sahin, M. A. Akkas, and O. Dagdeviren, "Low-cost and high-performance channel access strategies for internet of nano-things applications," *Future Gener. Comput. Syst.*, vol. 153, pp. 477–491, 2024.

[27] E. Sahin, O. Dagdeviren, and M. A. Akkas, "Energy-efficient hierarchical cluster-based routing strategies for internet of nano-things," *Ad Hoc Networks*, vol. 166, p. 103 673, 2025.

[28] J. Xu, X. Li, J. Kan, and R. Wang, "Energy harvesting-based thermal aware routing protocol for lung terahertz nanosensor networks," *Nano Commun. Networks*, vol. 43, p. 100 563, 2025.

©2026 The Author(s). This article is licensed under CC By 4.0